Moisture Ingress, Behavior, and Prediction Inside Semiconductor Packaging: A Review

Bongtae Han[1]
Department of Mechanical Engineering,
University of Maryland,
College Park, MD 20742
e-mail: bthan@umd.edu

Dae-Suk Kim
Department of Mechanical Engineering,
University of Maryland,
College Park, MD 20742

Reliability issues associated with moisture have become increasingly important as advanced electronic devices are nowhere more evident than in portable electronic products. The transition to the Pb-free solders, which require higher reflow temperature, makes the problem further exacerbated. Moisture absorbed into semiconductor packages can initiate many failure mechanisms, in particular interfacial delamination, degradation of adhesion strength, etc. The absorbed moisture can also result in catastrophic crack propagation during reflow process, the well-known phenomenon called popcorning. High vapor pressure inside pre-existing voids at material interfaces is known to be a dominant driving force of this phenomenon. This paper reviews various existing mechanisms of water accumulation inside voids. The procedures to obtain the critical hygroscopic properties are described. Advanced numerical modeling schemes to analyze the moisture diffusion phenomenon are followed with selected examples. [DOI: 10.1115/1.4035598]

Keywords: moisture diffusion, diffusivity, solubility, hygroscopic swelling, Fick's law, thermal–moisture analogy

1 Introduction

Due to its amorphous nature and topographical imperfection, polymeric materials always contain a large number of molecular scale voids inside them. This "free volume" is classically known to take 2.5% of the whole volume. Water and gas transport through those tiny free volume units present across polymer chain networks.

Nonpolar gases, such as O_2, N_2, CO_2, etc., penetrate through polymers by "jumping" from one void to another without causing considerable change of polymer structures. Polar water molecules, however, tend to form hydrogen bonding with polar groups in polymer chains (hydroxyl, amide, etc.) during diffusion through polymers. It results in structural, physical, and sometimes chemical changes in polymer structures such, as hydrolysis and hygroscopic swelling.

Semiconductor and micro-electromechanical systems (MEMS) packages have unique engineering structures. Various polymeric and inorganic materials are densely packed in millimeter to micrometer-scale configurations. Polymers such as molding compound, die attach, underfill, solder resist, etc., absorb moisture.

Water can reside inside polymer in three different states [1]. The first state is *nonfreezing water*; i.e., bound water that does not exhibit detectable phase transition that bulk water does. Absorbed water through hydrogen bonding in a diffusive way belongs to this state. The second state is *free water*, which has characteristics similar to bulk water. This state of water flows viscously inside polymer. The last state is *freezable bound water*; i.e., bound water whose phase transition temperatures are shifted due to interactions with polymer chains and/or capillary effects. Adsorbed water on void surfaces belongs to this state.

As shown in Ref. [1], a portion of water that initially migrates into a polymer becomes nonfreezing water (hydrogen bonding). After saturation, freezable bound water increases (adsorbed water portion). Then, free water starts to increase, if any. Most polymeric materials used in electronic packaging, however, are nonporous, and thus, this increase seldom occurs. The dominant water in electronic packaging materials is hydrogen-bonded water (nonfreezing bound) absorbed through bulk diffusion.

The absorbed moisture affects reliability in various ways. Accumulated moisture at bonded interfaces degrades the adhesion strength due to aging [2,3]. The absorbed moisture, unless properly removed by a baking process, generates internal high vapor pressure during solder reflow [4,5].

Polymers swell with the absorbed moisture [6,7]. Inorganic materials, such as silicon, copper, aluminum, etc., are impervious to moisture, and thus the volume does not change under the presence of moisture. This mismatch in hygroscopic swelling between the two material groups produces deformations, which are similar to the deformations induced by the mismatch of thermal expansion [7,8]. Various interconnect failures through popcorning and delamination are attributed to the combined effects; e.g., popcorn cracking in a plastic ball grid array (PBGA) package [9] and interconnection failure caused by hygroscopic swelling and adhesion degradation [10]. Many articles that address moisture-related failures are available in the literature [11–13] (numerous other articles are omitted due to space limitation).

Moisture diffusion in polymers had been a classical research topic [14]. The demand for modeling moisture-related phenomena in complex structures was more recently realized as moisture-related issues became critical to electronic package development [15]. This paper reviews various existing mechanisms of water accumulation inside voids. The procedures to obtain critical hygroscopic properties are described. Advanced numerical modeling schemes to analyze the moisture diffusion phenomenon are followed with selected examples.

2 Governing Equations

2.1 Moisture Diffusion. In general, diffusion of water molecules (moisture) into polymer chain structures follows Fick's

[1]Corresponding author.

Contributed by the Electronic and Photonic Packaging Division of ASME for publication in the JOURNAL OF ELECTRONIC PACKAGING. Manuscript received September 17, 2016; final manuscript received December 19, 2016; published online January 16, 2017. Assoc. Editor: Eric Wong.

laws. Mass flux in polymers is governed by Fick's first law, which is expressed as

$$J = -D \cdot \nabla C \tag{1}$$

where J is the moisture mass flux (kg/m^2 s), D is the diffusivity (m^2/s), ∇ is the gradient operator, and C is the moisture concentration (kg/m^3). The conservation of mass within an infinitesimal volume yields Fick's second law as

$$\dot{C} = \nabla \cdot (D \nabla C) \tag{2}$$

The equilibrium between saturated moisture concentration and ambient vapor pressure can be expressed as

$$C_{\text{sat}} = S \cdot p_v \tag{3}$$

where C_{sat} is the saturated moisture concentration, S is the solubility (s^2/m^2), and p_v is the ambient vapor pressure (Pa).

Equation (3) is based on the well-known Henry's law. For this reason, the solubility is often called as "Henry's coefficient" [16–18]. Henry's law described the partial pressure of a source solute in a gaseous state [19,20], and thus, the Henry's coefficient is valid only for solute-absorbent systems [19,20]. Equation (3) is an extended form of Henry's law to moisture–polymer systems, which has been known to be valid. In order to avoid any theoretical confusion, only "solubility" will be used in this paper.

Both the diffusivity and solubility are known to follow the Arrhenius relationship as

$$D = D_0 \exp\left(-\frac{E_D}{R_0 T}\right) \text{ and } S = S_0 \exp\left(-\frac{E_S}{R_0 T}\right) \tag{4}$$

where D_0 (m^2/s^2) and E_D (J/mol) are the constant and the activation energy of diffusivity, R_0 is the universal gas constant, S_0 and E_S are the constant (s^2/m^2) and the activation energy (J/mol) of solubility, and T is the temperature (K).

2.2 Analytical Solutions of Isothermal Diffusion Equation. Analytical solutions of Fick's second law are available for several single (homogeneous) material with simple geometry. For the isothermal one-dimensional (1D) problems illustrated in Fig. 1, the diffusion equation is reduced to

$$\frac{\partial C}{\partial t} = D \frac{\partial^2 C}{\partial x^2} \tag{5}$$

In Fig. 1, the one side of a polymer specimen is exposed to an ambient with an upstream vapor pressure (p_u), while the other side is impervious to moisture. It is also equivalent to a polymer specimen with a thickness of $2L$, both sides of which are exposed to a humid ambient. The boundary and initial conditions are

$$\frac{\delta C(0,t)}{\delta x} = 0,\ C(L,t) = C_u = Sp_u, \text{ and } C(x,0) = C_i = Sp_i \tag{6}$$

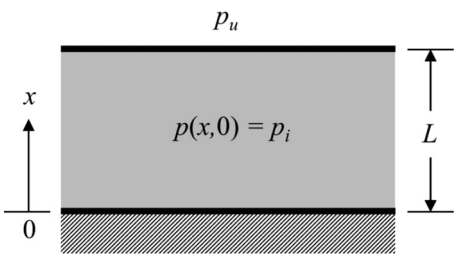

Fig. 1 Schematic illustration of 1D moisture diffusion

where C_u is the concentration at the top surface (kg/m^3), L is the thickness of the substrate (m), and C_i and p_i are the initial concentration and pressure, respectively. The closed-form analytical solution is expressed as [21]

$$C(x,t) = C_u - \sum_{n=1}^{\infty} \frac{4(C_i - C_u)}{(2n-1)\pi}(-1)^n \cos\frac{(2n-1)\pi x}{2L} \times \exp\left\{-\left[\frac{(2n-1)\pi}{2L}\right]^2 Dt\right\} \tag{7}$$

The moisture content inside the specimen is obtained by integrating the above solution as

$$\frac{m(t)}{m_{\text{sat}}} = 1 - \frac{8}{\pi^2}\sum_{n=1}^{\infty}\frac{1}{(2n-1)^2}\exp\left\{-\left[\frac{(2n-1)\pi}{2L}\right]^2 Dt\right\} \tag{8}$$

where m is the moisture content (kg) and m_{sat} is the saturated moisture content. The above solution can be easily extended to a three-dimensional (3D) block specimen subjected to moisture weight gain test, where all exterior surfaces of the block are exposed to a humid ambient. The solution of a 3D block specimen is given as [9]

$$\frac{m(t)}{m_{\text{sat}}} = 1 - \frac{512}{\pi^6}\sum_{l=1}^{\infty}\sum_{m=1}^{\infty}\sum_{n=1}^{\infty}\frac{1}{(2l-1)^2(2m-1)^2(2n-1)^2} \times \exp\left(-\frac{Dt}{L_{\text{eqv}}{}^2}\right) \tag{9}$$

where $L_{eqv}^2 = \{[(2l-1)\pi/L_x]^2 + [(2m-1)\pi/L_y]^2 + [(2n-1)\pi/L_z]^2\}^{-1}$ L_x, L_y, and L_z are the length of the block in each direction. Note that L_x in the 1D case is equal to $2L$. Equation (9) has been widely used to determine the diffusivity of block-shape polymer specimens inversely from experimentally measured moisture weight gain data.

2.3 Consideration for Multimaterial Systems. The moisture concentration is discontinuous at the interface between different polymeric materials. The maximum amount of moisture that each polymer can absorb is a material property, and thus, the concentration at a bimaterial interface becomes discontinuous.

A physical illustration of interfacial conditions is provided in Fig. 2, where $\boldsymbol{x}$ is any vector, that is, perpendicular to the interface

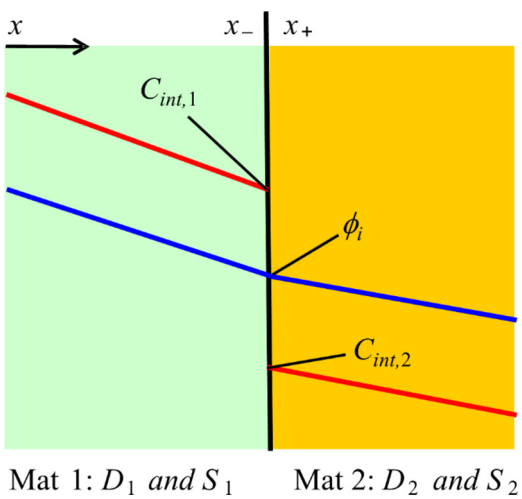

Fig. 2 Schematic illustration of moisture concentration at a bimaterial interface

Table 1 Constants and SI units

Term	Symbol	Unit
Mass concentration	C	kg/m^{-3}
Solubility	S	$s^2\ m^{-2}$
Normalized concentration	ϕ	Pa
Vapor pressure at ambient	p	Pa
Saturated vapor pressure	p_{sat}	Pa
Saturated concentration	C_{sat}	kg/m^{-3}
Mass flux	J	$kg/m^{-2}\ s^{-1}$
Mass diffusivity	D	$m^2\ s^{-1}$
Universal gas constant	R_0	$J\ mol^{-1}\ K^{-1}$

plane. The concentration at the interface is governed by the Nernst distribution law as [22]

$$\chi = \frac{C_{\text{int},1}}{C_{\text{int},2}} = \frac{S_1}{S_2} \tag{10}$$

where χ is Nernst partition coefficient at a specific temperature and $C_{\text{int},1}$ and $C_{\text{int},2}$ are concentrations of two materials at the interface. The corresponding mass continuity is given by

$$D_1 \frac{\partial C_1}{\partial x}\bigg|_{x-} = D_2 \frac{\partial C_2}{\partial x}\bigg|_{x+} \tag{11}$$

A new term, ϕ, in Fig. 2 is called "normalized concentration," which is defined to be C/S [16,17]. The normalized concentration will be discussed in Sec. 4.

The units of the moisture-related properties are not intuitive. Table 1 summarizes the constants and the corresponding SI units. It is worth noting that the normalized concentration has the unit of pressure. Although the unit is the same, the normalized concentration should not be confused with pressure.

3 Characterization of Hygroscopic Behavior

3.1 Diffusion Coefficient and Solubility. Two hygroscopic properties—diffusivity and solubility—are required in order to analyze moisture diffusion behavior quantitatively. They can be measured using the moisture weight gain/loss tests [23]. Property data for various packaging polymers are available in the literature [6,7,9,10,24–32] (numerous other articles are omitted due to space limitation). The majority of them were measured at low temperatures below 100 °C. A handful of property data at above 100 °C can be found in the literature [31,33]. More recently, an extensive experimental study on high-temperature measurements was conducted for more accurate modeling of moisture diffusion during reflow process [34,35].

Figure 3 shows moisture weight gain data obtained from two epoxy molding compounds (EMCs) at three different temperatures [34]. After the specimens were dried at 160 °C, they were subjected to a humid environment of 75%RH at three temperatures. An environmental chamber (ESPEC SH-241) was used to attain controlled humid environments. Moisture weight gain was measured periodically by a high precision balance (PI-225D, Denver Instrument, Bohemia, NY) until the measured weight of each sample remained unchanged for an extended period of time.

The moisture weight gain and the saturated weight gain in % wt. is defined as

$$w^{\%}(t)(\text{in \%wt.}) = 100 \times \frac{w(t) - w_{\text{dry@160°C}}}{w_{\text{dry@160°C}}} \text{ and } w^{\%}_{\text{sat}}(\text{in \%wt.}) = 100 \times \frac{w_{\text{sat}} - w_{\text{dry@160°C}}}{w_{\text{dry@160°C}}} \tag{12}$$

where w is the specimen weight gain (kg). The saturated weight gain, w_{sat}, is the maximum weight gain at the end of measurement.

The corresponding (average) moisture concentration and saturated concentration are given by

$$C(t) = w^{\%}(t)\frac{w_{\text{dry@160°C}}}{V_p} \text{ and } C_{\text{sat}} = w^{\%}_{\text{sat}}\frac{w_{\text{dry@160°C}}}{V_p} \tag{13}$$

where $w_{\text{dry@160°C}}$ and V_p are the polymer specimen mass and volume. Then, the solubility is determined from Eq. (3).

A nonlinear regression analysis was conducted to determine the diffusion coefficient at each temperature. The results from the regression are also shown in Fig. 3.

Equation (4) can be rewritten as

$$\ln D = (\ln D_0) - \left(\frac{E_D}{R_0}\right)\frac{1}{T} \text{ and } \ln S = (\ln S_0) - \left(\frac{E_S}{R_0}\right)\frac{1}{T} \tag{14}$$

Fickian diffusion coefficients obtained from three temperature data of Fig. 3 are plotted using Eq. (14). The results are shown in Fig. 4, where the slope represents the activation energy, E_D/R_0, of each material. The Fickian diffusivities followed the Arrhenius relationship well over the entire temperature range used in the study (45–85 °C). The constant and the activation energy of diffusivity were determined from the plots and they are summarized in Table 2.

The constant and the activation energy of solubility can be determined in a similar way. The solubility can be determined

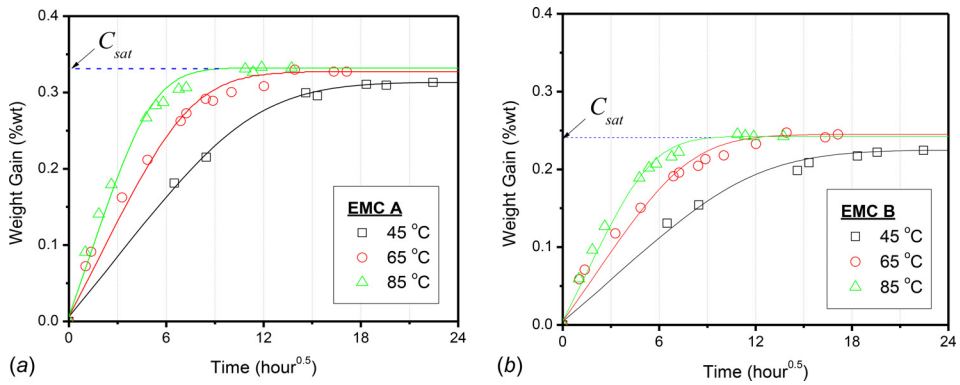

Fig. 3 Weight gain histories of: (*a*) EMC A and (*b*) EMC B, obtained at three temperatures and the humidity environment of 75%RH. Bullets and solid lines indicate the measurement data and corresponding Fickian curves, respectively.

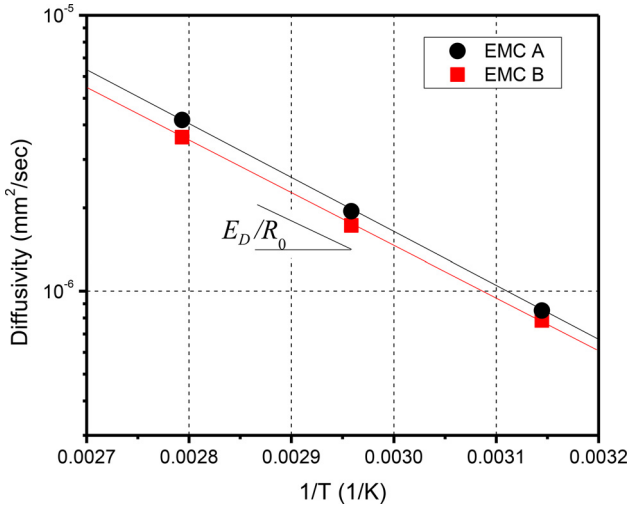

Fig. 4 Diffusivity versus temperature

Table 2 Diffusivity constants determined from absorption data [34]

Absorption	EMC A	EMC B
D_0 (mm²/s)	1.04	0.674
E_D (J/mol)	37,294	36,145
D_{0C}	3.9	2.5
a (m³/kg)	−0.28	−0.28

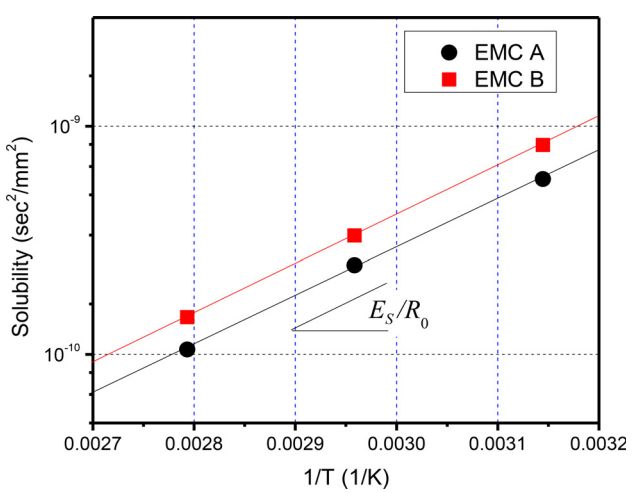

Fig. 5 Solubility versus temperature

Table 3 Solubility constants determined from experimental data [34]

Below T_g	S_0 (s²/mm²)	E_S (J/mol)
EMC A	2.17×10^{-17}	−46,352
EMC B	2.54×10^{-17}	−45,020

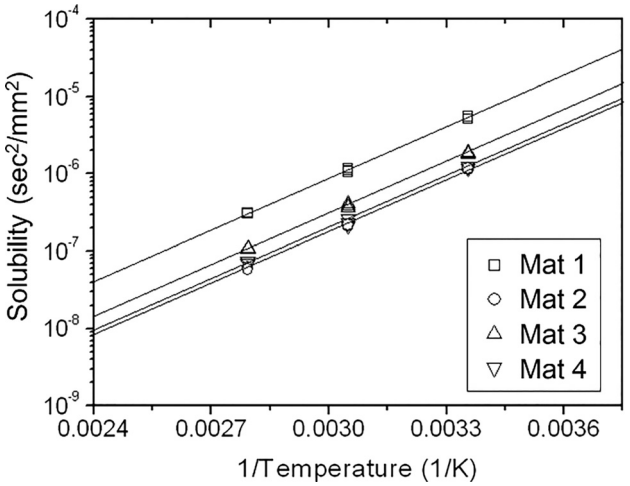

Fig. 6 Solubility versus temperature obtained from four different packaging materials

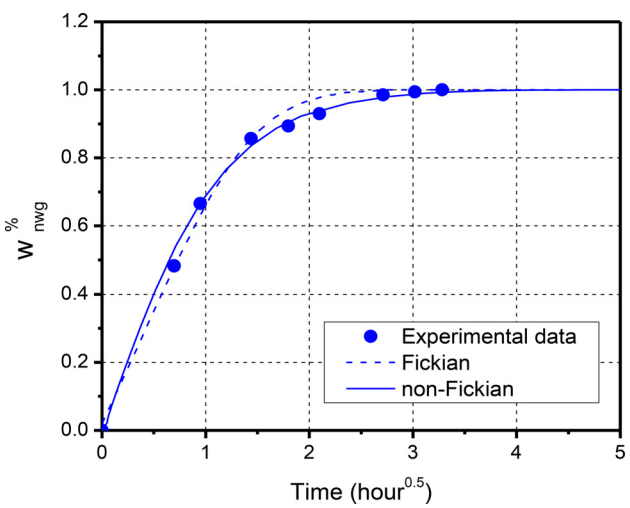

Fig. 7 Fickian and non-Fickian solutions are compared with experimental data of EMC A obtained at 180 °C

from the saturated concentrations marked in Fig. 3. The values are plotted in Fig. 5 using Eq. (14). The solubility also followed the Arrhenius relationship well over the entire temperature range. The constant and the activation energy of solubility were determined from the plots and they are summarized in Table 3.

Wong et al. [31,33] first reported that the activation energy for the solubility of the packaging materials ranges from −44,000 to −46,000 J/mol. The results imply that there is no strong correlation between the saturated concentration and the temperatures below 100 °C [18,31,33]. A similar trend was observed for both specimens.

More evidence is shown in Fig. 6, where the solubility versus temperature values obtained from four different materials are plotted [18]. As mentioned earlier, the slope represents the activation energy, E_s/R_0, of each material. The slopes are nearly identical, which indicates a nearly constant value of the activation energy.

3.1.1 Non-Fickian Diffusivity. Some polymers show non-Fickian behavior. Two approaches to model non-Fickian gas diffusion are available in the literature: dual-sorption theory [36] and concentration-dependent diffusivity [37].

A typical non-Fickian behavior with normalized weight gain ($w^{\%}_{nwg}$) is shown in Fig. 7, which was obtained from an EMC at 180 °C [34]. A modified approach to obtain a diffusivity equation as a function of both temperature and concentration was proposed, where the Arrhenius equation was combined with the concentration dependency [34]. It is expressed as

$$D = D_0 D_{0C} \exp\left(\frac{E_D}{R_0 T} + aC\right) \tag{15}$$

where D_{0C} is a dimensionless adjustment coefficient for concentration dependence and a is the exponent constant relevant to concentration dependence. Accordingly, the diffusion equation can be modified as

$$\frac{\partial C}{\partial t} = \nabla \cdot \left[D_0 D_{0C} \exp\left(\frac{E_D}{R_0 T} + aC\right) \nabla C \right] \tag{16}$$

The constant, a, represents the degree of concentration dependency of the diffusivity. It governs the magnitude of discrepancies between Fickian curves and experimental data. Since the diffusivity monotonically changes with the concentration from unity at $C = 0$ to $e^{aC_{sat}}$ at $C = C_{sat}$, weight gain can be accelerated or retarded depending on the sign of a. Such a biased change is adjusted by another constant D_{0C}.

Using the Fickian constants (D_0 and E_D), nonlinear regression analyses were repeated to determine the values of a and D_{0C}. Since an analytical solution of Eq. (16) was not available, a finite-element model based on a thermal–moisture analogy was implemented to solve the non-Fickian diffusion problem using ANSYS [17,34]. The constants determined through this procedure are listed in Table 2. The weight curve using the four constants is also plotted in Fig. 7 along with the Fickian curve. A better fit over the entire history was resulted.

3.2 Hygroscopic Swelling Coefficient. The polar water molecules form hydrogen bonds with the hydroxyl groups in the polymer chains and disrupt interchain hydrogen bonding. These water molecules increase the intersegmental hydrogen bond length and collectively cause the polymeric material to swell. This dimensional increase due to the absorption of moisture is called hygroscopic swelling. The hygroscopic strain is known to have a linear relationship with moisture concentration as [7]

$$\varepsilon_h = \beta \cdot \Delta C \tag{17}$$

where ε_h is the hygroscopic strain and β is the coefficient of hygroscopic swelling (CHS). ΔC is the moisture concentration difference.

The CHS can be measured by various tools and techniques including a bending cantilever method [38], a micrometer [39], Michelson interferometry [40], and thermomechanical analyzer (TMA) combined with thermogravimetric analyzer (TGA) [6]. A full-field deformation analysis can be used to cope with the limitation of point-measurement methods. Moiré interferometry [41] and digital image correlation (DIC) [42] have been utilized for hygroscopic swelling strains in bulk polymers [43] and thin film polymers [44], respectively. The CHS measurement using moiré interferometry is reviewed here.

The overview of the experimental procedure is illustrated in Fig. 8 [7]. Two samples of a material of interest were first baked to remove any initial moisture content (a). After the bake is completed, cross-line diffraction gratings were replicated onto the samples at an elevated temperature of 85 °C using a high-temperature curing epoxy (Tra-Con Tra-Bond F230) (b). One of the two samples (reference sample) was left in the baking oven to ensure no extra moisture gain (c). The second sample (test sample) was subjected to an 85 °C/85%RH environment and its weight was periodically monitored until a saturation state was reached (d). Once the saturation state was achieved, the hygroscopic swelling measurement was performed by moiré interferometry during desorption process (e).

It was vital to eliminate thermal expansion during moiré measurements so that only hygroscopic swelling was documented. This was accomplished by using the reference sample. The reference and test samples are positioned side by side during measurements.

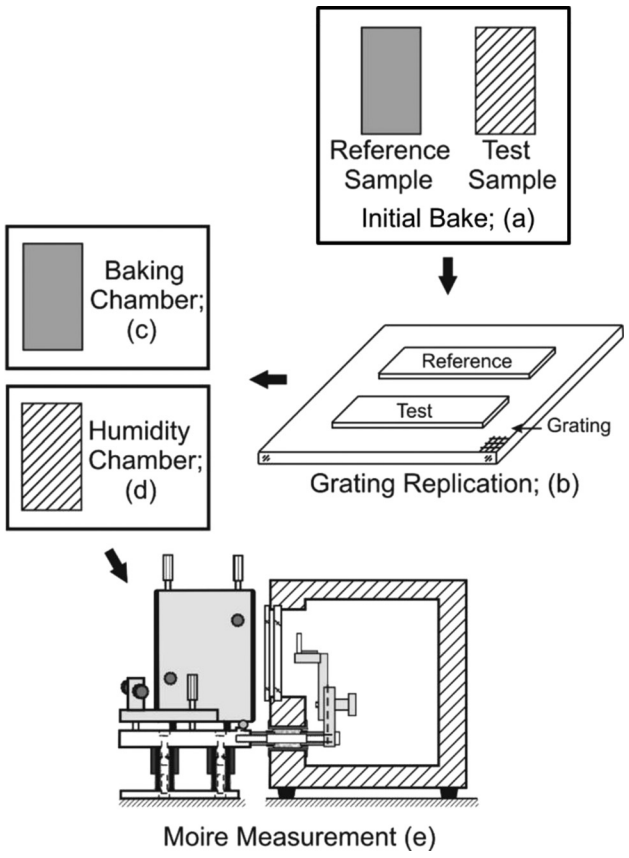

Fig. 8 Overview of CHS measurement procedure using moiré interferometry

The interferometer was first tuned to produce a null field (devoid of fringes) on the reference sample and the test sample was viewed subsequently. This procedure canceled any thermally induced deformations in the test sample since the deformed state of the reference sample was used as a reference datum for zero hygroscopic deformation of the test sample.

The null field fringe pattern obtained from the reference sample is shown in Fig. 9(*a*). The representative fringe patterns of the test sample obtained right after saturation ($t = 0$) and after 40 h are shown in Figs. 9(*b*) and 9(*c*), respectively. The hygroscopic strain, ε_h, can be determined directly from moiré fringe patterns by

$$\varepsilon_h = \frac{1}{2f_s}\frac{\Delta N}{\Delta L} \tag{18}$$

where f_s is the frequency of the specimen grating (1200 lines/mm), ΔN is the change of fringe orders in the moiré pattern, and ΔL is any gage length across which ΔN is determined. The hygroscopic strains are plotted against moisture content (%) in Fig. 10. It is evident that a linear relationship exists between hygroscopic swelling and moisture content. The slope is the CHS value of the material ($\beta = 0.27$).

4 Modeling of Moisture Diffusion

Commercially available software packages are preferred choices to solve the diffusion problems of semiconductor/MEMS packages as they typically have complex geometries, material configurations, and loading conditions. Not all commercial finite-element analysis (FEA) software packages offer the moisture (or mass) diffusion function [17]. Furthermore, when moisture transport into/out of a cavity is involved, the modeling task becomes

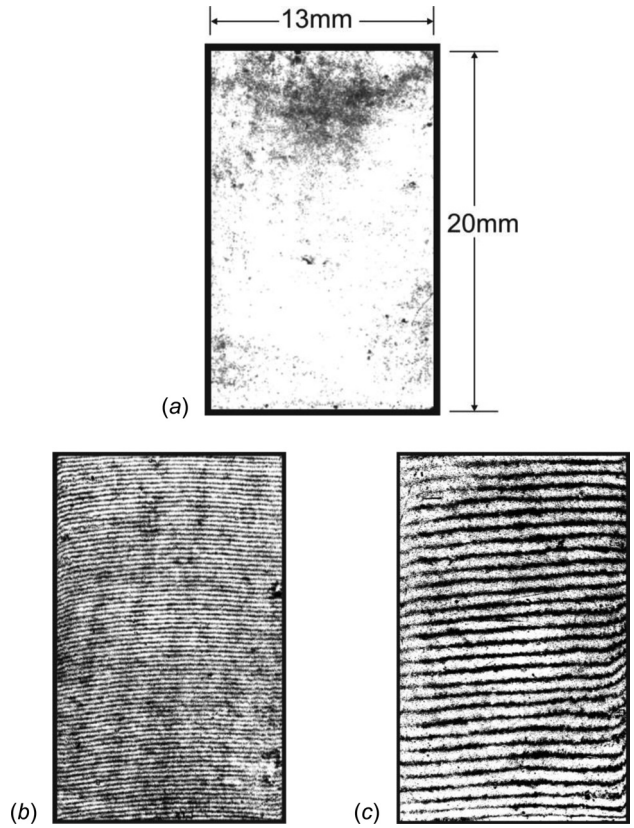

Fig. 9 Moiré fringe patterns: (*a*) null fields obtained from the reference sample; fringe patterns of the test sample at time intervals of (*b*) zero and (*c*) 40 h

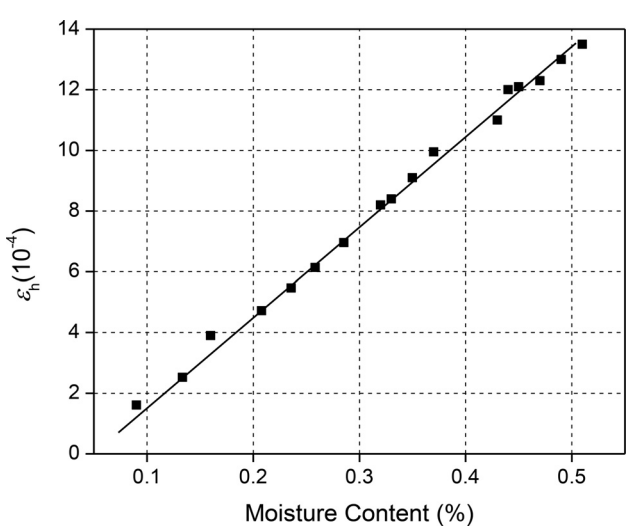

Fig. 10 Hygroscopic strain versus moisture content (%) obtained from moiré fringes

even more complicated. This section presents numerical schemes to handle the two issues effectively.

4.1 Thermal–Moisture Analogy. Heat conduction is a diffusive process and thus has a governing equation similar to that of mass diffusion. Fourier's law of heat conduction is expressed as

$$q = -k\nabla T \tag{19}$$

where q is the heat flux (W/m^2), T is the temperature (K), and k is the conductivity (W/m K). Assuming no internal heat generation, the energy balance yields the governing equation of heat conduction as

$$\dot{T} = \nabla \cdot (\alpha \nabla T) \text{ or } \rho c_p \dot{T} = \nabla \cdot (k \nabla T) \tag{20}$$

where α is the thermal diffusivity (m^2/s) and ρ and c_p are the density (kg/m^3) and the specific heat (J/kg K), respectively.

Due to the similarity in governing equations (Eqs. (2) and (20)), heat conduction and mass diffusion have been often treated in a "unified" way [45]. The resulting "thermal–moisture" analogy is very attractive, since moisture diffusion can be solved using the heat transfer function of any FEA software. As a consequence, the thermal–moisture analogy has been utilized extensively to address water diffusion inside semiconductor packages [9,10,46], food [47], and gas barrier films [48,49].

4.1.1 Direct Analogy. For a homogenous and isotropic material, a thermal–moisture analogy can be established from direct comparison between Eqs. (2) and (20) [17]. This direct analogy can be expressed as

$$\begin{aligned} &\text{Field variable}: T\,(\text{temperature}) \equiv C\,(\text{concentration}) \\ &\text{Diffusivity}: \alpha\,(\text{thermal}) \equiv D\,(\text{moisture}) \end{aligned} \tag{21}$$

The direct analogy scheme is simple, but this analogy is applicable to only single-material or homogeneous problems; it cannot handle the interface discontinuity that occurs in multimaterial problems [17].

4.2 Multimaterial Problems. The moisture concentration is discontinuous at a bimaterial interface as mentioned earlier. In order to make this problem numerically possible, normalized field variables are introduced, which are continuous across the material interfaces.

4.2.1 Normalized Analogy. A normalized concentration is defined as [17]

$$\phi = \frac{C}{S} \tag{22}$$

where ϕ is normalized concentration (Pa). Substituting Eq. (22) into Eq. (2), Fick's equation yields

$$\frac{\partial(S\phi)}{\partial t} = \nabla \cdot [D\nabla(S\phi)] \Rightarrow \dot{S}\phi + S\dot{\phi} = \nabla \cdot [D\nabla(S\phi)] \tag{23}$$

The corresponding boundary condition at the exterior surface is given from Eq. (3) as

$$\phi_{\text{BC}} = p_v \tag{24}$$

When $\nabla S = \dot{S} = 0$, the solubility is constant and Eq. (23) becomes

$$S\dot{\phi} = \nabla \cdot [(DS)\nabla\phi] \tag{25}$$

Then, the normalized analogy can be established by comparing Eqs. (25) to (20) as

$$\begin{aligned} \text{Field variable}: \quad T &\equiv \phi \\ k &\equiv DS \\ \rho c_p &\equiv S \end{aligned} \tag{26}$$

It is important to note that S should be included in the normalized analogy; if the analogy is set as $\rho c_p \equiv 1$ and $K \equiv D$, the mass continuity (Eq. (11)) will not be satisfied.

The above analogy should properly handle the interface condition as the field variable is the concentration normalized by

solubility which is continuous at the material interface. It is important to remember, however, that the normalized analogy was established for the condition of constant solubility; the temperature distribution must be uniform ($\nabla S = 0$) and independent of time ($\dot{S} = 0$), since solubility is a temperature-dependent property. This condition is met only when the loading is isothermal, and thus, the normalized analogy should be applied only to isothermal problems.

The normalized concentration, ϕ, is often referred to as the "activity" of the diffusing material [16], which provides the physical meaning of the normalized concentration using the dissociation of a diatomic gas during diffusion. Equilibrium requires the partial pressure to be continuous across an interface, and thus, the normalized concentration will be continuous as well. Galloway and Miles [9] used a similar argument and called the normalized concentration *moisture partial pressure*, P, and used the following expression, which is basically identical to Eq. (22):

$$P = \frac{C}{S} \tag{27}$$

It is important to note that the moisture partial pressure, P, is just a symbol for solution variable and should not be confused with either the ambient vapor pressure, p_v, or the chemical potential inside a polymer, which usually defined in terms of Gibbs free energy [50].

An alternate normalized variable, W, called *relative concentration* or *wetness*, was introduced by Puig et al. [51] and later Wong et al. [52–56]. It is defined as

$$W = \frac{C}{C_{\text{sat}}} \tag{28}$$

Under the assumption that solubility remains constant regardless of the level of concentration, the wetness can be expressed as

$$W = \frac{\phi}{p_v} \tag{29}$$

It is clear from the above equation that the two normalized variables are basically the same since the ambient vapor pressure, p_v, is constant at a given temperature.

The term *moisture partial pressure* implies the vapor phase of water, while the concept of *wetness* does the liquid phase of water. In fact, water diffused into a solid exists as water molecules and its phase can change by numerous conditions. Regardless of the phase, however, the physical meaning of the normalized variables is nothing more than normalized concentration for the case of moisture diffusion. Consequently, the normalized concentration or wetness yields identical result when the analogy is implemented to determine the moisture concentration.

4.2.2 Advanced Analogy. The advanced analogy scheme was proposed to cope with the limitations of the normalized analogy [18]. It was established based on the unique behavior of the most commonly used packaging polymers that the saturated concentration is linearly proportional to the ambient relative humidity but not dependent on the temperature.

The experimental evidence of the behavior is shown in Fig. 11, where the saturated moisture concentrations obtained at 25 °C, 55 °C, and 85 °C are plotted as a function of relative humidity. It clearly shows that there exists a linear relationship between the saturated concentration and the relative humidity over the temperature range used in the measurements (below the glass transition temperature of the polymer). This behavior has been observed in numerous other studies [31,42,50,52,57–60].

The linear relationship between the saturated concentration and the relative humidity can be expressed as

$$C_{\text{sat}} = S \cdot p_v = S \cdot p_{\text{sat}} \cdot \text{RH}\% = M \cdot \text{RH}\% \tag{30}$$

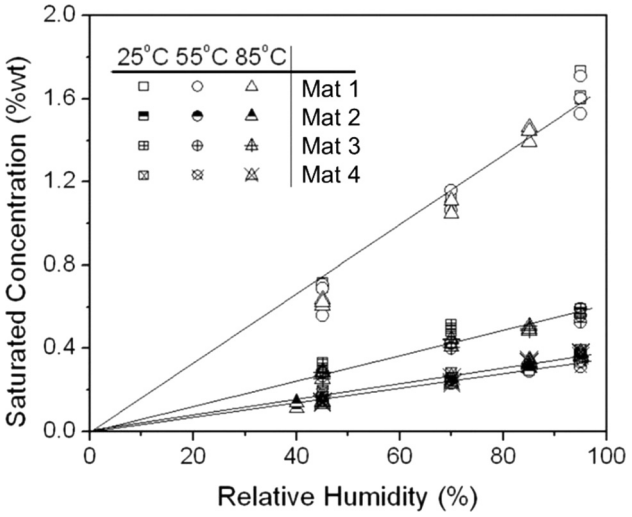

Fig. 11 Saturated concentration of various packaging polymers versus relative humidity

where p_{sat} is the saturated vapor pressure (Pa), RH% is the relative humidity, and M is the "modified solubility," which is a temperature-independent material property.

The advanced analogy uses the modified solubility. An advanced normalized concentration, φ, is defined using the modified solubility as

$$\varphi = \frac{C}{M} \tag{31}$$

Substituting Eq. (31) into Eq. (2) yields

$$\dot{M}\varphi + M\dot{\varphi} = \nabla[D\nabla(M\varphi)] \Rightarrow M\dot{\varphi} = \nabla[DM\nabla\varphi] \tag{32}$$

Thus, the advance analogy is established by comparing Eq. (32) with Eq. (20) as

$$\begin{aligned} \text{Field variable}: \quad T &\equiv \varphi \\ k &\equiv MD \\ \rho c_p &\equiv M \end{aligned} \tag{33}$$

The modified solubility automatically satisfies the mass continuity at the interface. The boundary condition of the new normalized concentration becomes ambient relative humidity (RH%), i.e.,

$$\varphi_{\text{BC}} = \text{RH}\% \tag{34}$$

The above derivation clearly indicates that the advanced analogy is valid for multimaterial systems subjected to anisothermal loading conditions (nonuniform temperature fields that change with time).

It is important to note that temperature-independent linear relationship between the saturated moisture concentration and the relative humidity may not exist above the glass transition temperature as well as for polymer composites [61–64]. The temperature-independent linearity must be confirmed experimentally to utilize the proposed scheme accurately.

4.2.3 Validation of Analogies. The three analogy schemes are summarized in Table 4. They were validated by numerically solving the original diffusion equation, Eq. (2) [17,18,57].

The validity of the normalized concentration was verified first [17,57]. As illustrated in Fig. 12(*a*), the simulation considered moisture diffusion in a 0.2 mm-thick double-layered wall. For an

Table 4 Summary of three analogy schemes

Thermal	Direct	Normalized	Advanced
T	C	ϕ	φ
K	D	$D{\cdot}S$	$D{\cdot}M$
ρc_p	1	S	M
BC	C_{sat}	p_v	RH%
Multimaterial	X	O	O
Anisothermal	O	X	O

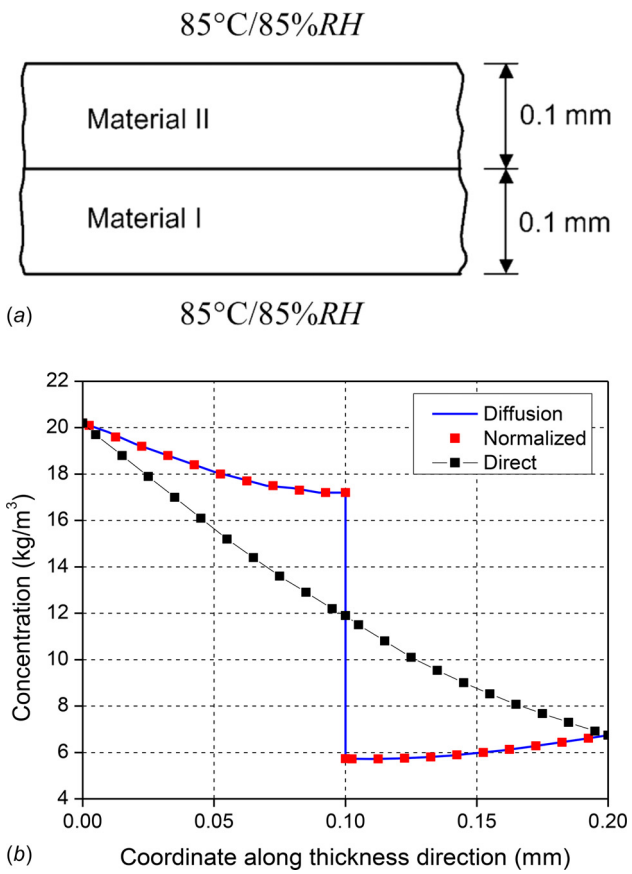

Fig. 12 Implementation of normalized analogy: (*a*) bimaterial specimen subjected to an isothermal loading condition and (*b*) distribution of moisture concentration at $t = 3600$ s

isothermal loading condition, the wall was exposed to a relative humidity of 85%RH at an ambient temperature of 85 °C.

The distribution of moisture concentration obtained from the direct and normalized analogy schemes are shown in Fig. 12(*b*) [17,57], where the results are compared with the results of the diffusion analysis. The normalized analogy handles the bimaterial problem effectively and produces a correct distribution of moisture, where the discontinuity of moisture concentration at the interface is evident.

The validity of the advanced analogy was also verified using a bimaterial structure subjected to anisothermal loading [18]; the loading incorporated not only temperature change with time ($\dot{T} \neq 0$, and thus $\dot{S} \neq 0$) but also spatially nonuniform temperature distribution ($\nabla T \neq 0$, and thus $\nabla S \neq 0$).

The configuration of the structure and loading conditions are illustrated in Fig. 13(*a*). The problem was solved by the normalized and advanced analogies. The results at $t = 3600$ s are plotted in Fig. 13(*b*) together with the solution of the diffusion equation. The advanced analogy scheme predicted the moisture concentration accurately, while the normalized analogy significantly

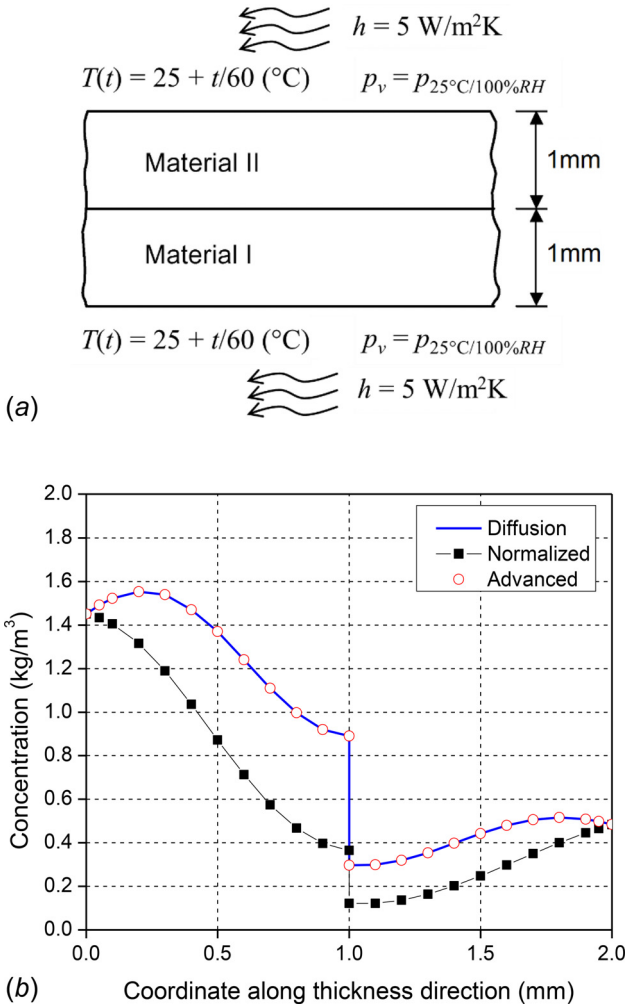

Fig. 13 (*a*) Schematic diagram of simulated geometry and boundary condition for the anisothermal bimaterial case and (*b*) moisture concentrations at $t = 3600$ s

deviated from the solution. The results confirmed that the advanced analogy is applicable to all anisothermal cases.

4.3 Moisture Transport for MEMS Cavity. MEMS devices have an internal cavity for moving parts and proper packaging should be provided to maintain the internal condition of the cavity. The cavity is formed by sealing a gap between cap and substrate wafers. Hermeticity of MEMS packages is a measure of the ability to maintain an acceptable level of stable and sometimes inert ambient in the cavity. Good hermeticity is essential for compliance with performance and reliability standards [65].

The most commonly used sealing materials to provide hermeticity are low-melting point eutectics, such as AuSn, AuSi, and other tin-based alloys. More recently, polymers have gained widespread acceptance due to many advantages that they offer [66,67]. Examples of polymeric seals include benzocyclobutene (BCB), parylene, polyimide, and negative photoresists [68,69]. Modeling of moisture transport into and out of a cavity through a polymeric seal is crucial in assessment of hermeticity performance of polymer-sealed MEMS packages.

Assuming that water vapor obeys the ideal gas law, the cavity vapor pressure by moisture transport through polymeric seals can be determined by

$$p_c(t_1) = p_c(0) + \frac{R_0 T}{M_w V_c} \int_{t_1} \int_{A_c} J_c(t) \cdot dA dt \tag{35}$$

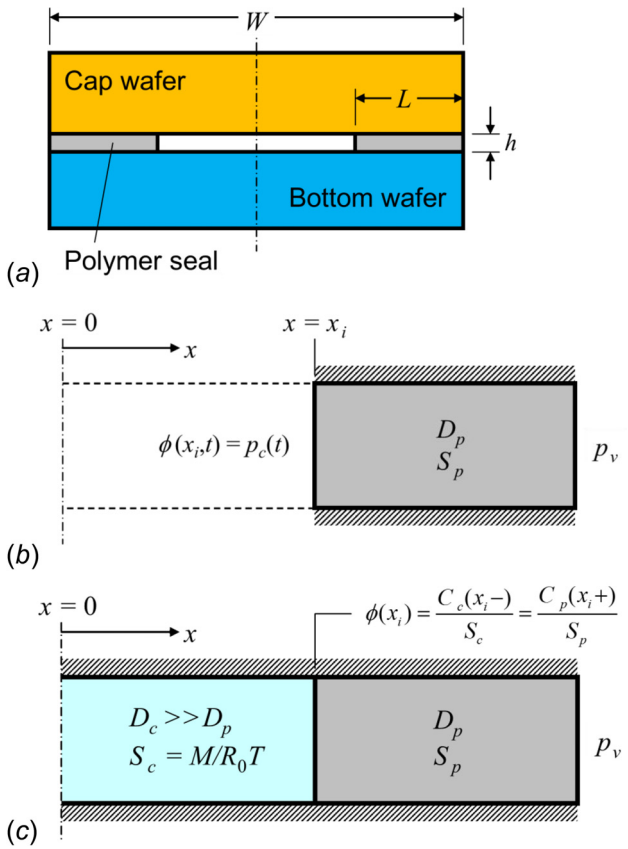

Fig. 14 Schematic illustration of: (*a*) cross section of MEMS devices; and (*b*) "original" model and (*c*) effective volume model in a simplified 1D configuration [65]

where p_c is the cavity pressure (Pa), M_w is the molar mass of water (0.018 kg/mol), V_c is the cavity volume (m^3), A_c is the total area of polymeric seal surfaces in the cavity, and J_c is the moisture mass flux into the cavity (kg/m^2 s) through polymeric seals.

A 3D package (Fig. 14(*a*)) can be modeled as a two-dimensional (2D) structure (Fig. 14(*b*)) since a cavity and a seal are sandwiched by a silicon chip through which gas cannot penetrate. The 2D diffusion model can be solved numerically by commercially available FEA software packages. It is important to recall that the boundary condition at the polymer seal and cavity interface is transient; the cavity pressure increment at each time step should be calculated and subsequently used to update the boundary condition at the inner surface after each time step. This updating process requires a user-defined algorithm (this scheme is referred to as "the original" scheme). An effective modeling scheme was proposed to cope with the problem (this scheme is referred to as "effective volume") [65].

A schematic illustration of the effective volume scheme is shown in Fig. 14(*c*). It modeled the package cavity as a fictitious polymer with an extremely large diffusivity and an "equivalent solubility." The large diffusivity ensured the uniform vapor pressure inside the cavity. It is important to note, however, that the solubility of the fictitious polymer cannot be chosen arbitrary. Instead, the effective solubility should be derived from the gas law and Henry's law as

$$S_c = \frac{C}{p} = \frac{\rho}{nR_0T/V} = \frac{M_w}{R_0T} \tag{36}$$

where ρ, V, and n are the water vapor density (kg/m^3), the volume (m^3) of the cavity, and the number of moles (mol). Note that the water vapor density has the same dimension as the moisture concentration and it can be interpreted as moisture concentration inside the imaginary polymer.

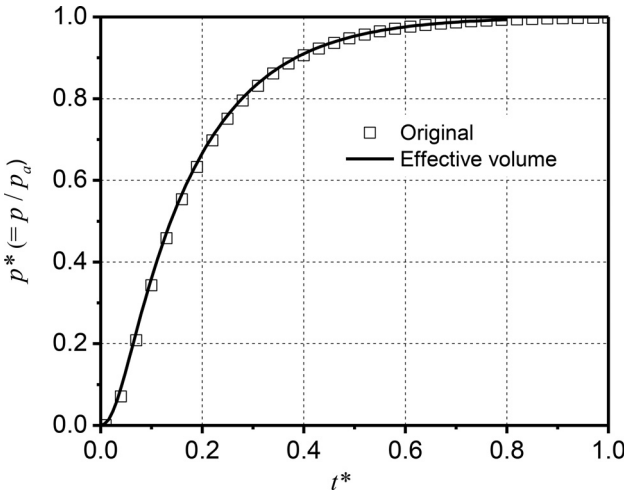

Fig. 15 Normalized pressure inside cavity as a junction of normalized time

The effective volume scheme transforms the original single material diffusion problem with transient boundary conditions into a bimaterial gas diffusion problem with fixed boundary conditions. Consequently, the Nernst distribution law should be considered for mass continuity at the cavity–polymer seal interface (the inner surface of the polymer seal, $x = L$ in Fig. 14(*b*), which can be expressed as [22]

$$\phi(L) = p(L) = \frac{C_c(L-)}{S_c} = \frac{C_p(L+)}{S_p} \tag{37}$$

where C_c and C_p is the moisture concentration of the cavity and the polymer seal, respectively.

In the effective volume scheme, the mass continuity is automatically satisfied at the interface, and thus, the interface condition does not have to be updated manually. As a results, the commercial FEA software packages can be employed to implement the effective volume scheme with either normalized or advanced analogy. It is important to note, however, that only isothermal cases should be solved even when the advanced analogy is employed, because Eq. (36) is not valid for general anisothermal cases.

The effective-volume scheme was validated with the original scheme. In the validation, a simple 1D axisymmetric geometry was considered, which simulated an MEMS device with a cavity at the center [70]. Since no closed-form solution was available for the original schemes, it was solved by a numerical scheme based on the finite-difference method (FDM) [71].

Figure 15 shows cavity pressure evolution as a function of time for the case, where the seal width and the inner cavity radius are the same [70]. The two schemes produce identical curves, confirming the validity of the effective volume scheme. Validation with experimental data can be also found in Refs. [65,72].

5 Summary

Fundamentals of moisture transport inside semiconductor packaging were reviewed. The procedures to obtain critical hygroscopic properties (diffusivity, solubility or saturated concentration, and hygroscopic swelling coefficient) were established well for the past decades, and abundant data were available in the literature. However, most of the data were obtained below 100 °C and under RH less than 85%, and the data above the water boiling temperature were still limited in the literature. More experiments

to measure the data above 100 °C as well as at RH of 100% are warranted to provide complete understanding about the moisture behavior during solder reflow after preconditioning.

Numerical modeling schemes for diffusion analyses of packaging structures were developed for the last two decades and have been used extensively for various moisture transport problems including MEMS devices containing an internal cavity. The thermal analogy schemes are convenient and effective for the diffusion analysis, but cautions must be given to their applicable domains when implemented for diffusion problems with complex geometries and loading conditions.

Acknowledgment

This work was supported by the Center for Advanced Life Cycle Engineering (CALCE) of the University of Maryland. Their support is gratefully acknowledged. The authors wish to thank the reviewers for their critical and careful review.

References

[1] Hodge, R. M., Edward, G. H., and Simon, G. P., 1996, "Water Absorption and States of Water in Semicrystalline Poly(Vinyl Alcohol) Films," Polymer, **37**(8), pp. 1371–1376.
[2] Tanaka, N., Kitano, M., Kumazawa, T., and Nishimura, A., 1999, "Evaluating IC-Package Interface Delamination by Considering Moisture-Induced Molding-Compound Swelling," IEEE Trans. Compon. Packag. Technol., **22**(3), pp. 426–432.
[3] Gektin, V., and Bar-Cohen, A., 1996, "Mechanistic Figures of Merit for Die-Attach Materials," Inter-Society Conference on Thermal Phenomena in Electronic Systems, (ITHERM V), Orlando, FL, May 29–June 1, pp. 306–313.
[4] Kitano, M., Nishimura, A., Kawai, S., and Nishi, K., 1988, "Analysis of Package Cracking During Reflow Soldering Process," 26th Annual IEEE International Reliability Physics Symposium, Monterey, CA, Apr. 12–14, pp. 90–95.
[5] Wang, Z., 2011, "Vapour Pressure Modelling for Plastic Encapsulated Microelectronics Subjected to Lead-Free Solder Reflow Profile," Strain, **47**(s1), pp. e148–e155.
[6] Ardebili, H., Ee Hua, W., and Pecht, M., 2003, "Hygroscopic Swelling and Sorption Characteristics of Epoxy Molding Compounds Used in Electronic Packaging," IEEE Trans. Compon. Packag. Technol., **26**(1), pp. 206–214.
[7] Stellrecht, E., Han, B., and Pecht, M. G., 2004, "Characterization of Hygroscopic Swelling Behavior of Mold Compounds and Plastic Packages," IEEE Trans. Compon. Packag. Technol., **27**(3), pp. 499–506.
[8] Yoon, S., Jang, C., and Han, B., 2008, "Nonlinear Stress Modeling Scheme to Analyze Semiconductor Packages Subjected to Combined Thermal and Hygroscopic Loading," ASME J. Electron. Packag., **130**(2), p. 024502.
[9] Galloway, J. E., and Miles, B. M., 1997, "Moisture Absorption and Desorption Predictions for Plastic Ball Grid Array Packages," IEEE Trans. Compon., Packag., Manuf. Technol.: Part A, **20**(3), pp. 274–279.
[10] Tee, T. Y., and Zhong, Z., 2004, "Integrated Vapor Pressure, Hygroswelling, and Thermo-Mechanical Stress Modeling of QFN Package During Reflow With Interfacial Fracture Mechanics Analysis," Microelectron. Reliab., **44**(1), pp. 105–114.
[11] Zhang, G. Q., van Driel, W. D., and Fan, X. J., 2006, *Mechanics of Microelectronics*, Springer, Dordrecht, The Netherlands.
[12] Fan, X. J., Zhang, G. Q., Driel, W. D. V., and Ernst, L. J., 2008, "Interfacial Delamination Mechanisms During Soldering Reflow With Moisture Preconditioning," IEEE Trans. Compon. Packag. Technol., **31**(2), pp. 252–259.
[13] Shi, X. Q., Zhang, Y. L., Zhou, W., and Fan, X. J., 2008, "Effect of Hygrothermal Aging on Interfacial Reliability of Silicon/Underfill/FR-4 Assembly," IEEE Trans. Compon. Packag. Technol., **31**(1), pp. 94–103.
[14] Lee, M. C., and Peppas, N. A., 1993, "Water Transport in Graphite/Epoxy Composites," J. Appl. Polym. Sci., **47**(8), pp. 1349–1359.
[15] Kitano, M., Kawai, S., Nishimura, A., and Nishi, K., 1989, "A Study of Package Cracking During the Reflow Soldering Process," Trans. Jpn. Soc. Mech. Eng., Ser. A, **55**(510), pp. 356–363.
[16] Dassault Systèmes, 2012, "ABAQUS 6.12, Theory Manual," Dassault Systèmes, Providence, RI, accessed Sept. 14, 2016, http://abaqus.software.polimi.it/v6.12/books/stm/default.htm
[17] Yoon, S., Han, B., and Wang, Z., 2007, "On Moisture Diffusion Modeling Using Thermal-Moisture Analogy," ASME J. Electron. Packag., **129**(4), pp. 421–426.
[18] Jang, C., Park, S., Han, B., and Yoon, S., 2008, "Advanced Thermal-Moisture Analogy Scheme for Anisothermal Moisture Diffusion Problem," ASME J. Electron. Packag., **130**(1), p. 011004.
[19] Henry, W., 1803, "Experiments on the Quantity of Gases Absorbed by Water, at Different Temperatures, and Under Different Pressures," Philos. Trans. R. Soc. London, **93**(0), pp. 29–276.
[20] Wong, E. H., 2015, "The Fundamentals of Thermal-Mass Diffusion Analogy," Microelectron. Reliab., **55**(3–4), pp. 588–595.
[21] Gebhart, B., 1993, *Heat Conduction and Mass Diffusion*, McGraw-Hill, New York.
[22] Jost, W., 1960, *Diffusion in Solids, Liquids, Gases*, 3rd ed., Academic Press, New York.
[23] JEDEC, 2001, "Test Method for the Measurement of Moisture Diffusivity and Water Solubility in Organic Materials Used in Electronic Devices," JEDEC Solid State Technology Association, Arlington, VA, Standard No. 22-A120A.
[24] Fan, X. J., Lee, S. W. R., and Han, Q., 2009, "Experimental Investigations and Model Study of Moisture Behaviors in Polymeric Materials," Microelectron. Reliab., **49**(8), pp. 861–871.
[25] Xie, B., Fan, X. J., Shi, X. Q., and Ding, H., 2009, "Direct Concentration Approach of Moisture Diffusion and Whole-Field Vapor Pressure Modeling for Reflow Process—Part I: Theory and Numerical Implementation," ASME J. Electron. Packag., **131**(3), p. 031010.
[26] Xie, B., Fan, X. J., Shi, X. Q., and Ding, H., 2009, "Direct Concentration Approach of Moisture Diffusion and Whole-Field Vapor Pressure Modeling for Reflow Process—Part II: Application to 3D Ultrathin Stacked-Die Chip Scale Packages," ASME J. Electron. Packag., **131**(3), p. 031011.
[27] Placette, M. D., Fan, X. J., Zhao, J.-H., and Edwards, D., 2012, "Dual Stage Modeling of Moisture Absorption and Desorption in Epoxy Mold Compounds," Microelectron. Reliab., **52**(7), pp. 1401–1408.
[28] Chen, L., Chu, H.-W., and Fan, X. J., 2015, "A Convection–Diffusion Porous Media Model for Moisture Transport in Polymer Composites: Model Development and Validation," J. Polym. Sci., Part B: Polym. Phys., **53**(20), pp. 1440–1449.
[29] Chen, L., Adams, J., Chu, H.-W., and Fan, X. J., 2016, "Modeling of Moisture Over-Saturation and Vapor Pressure in Die-Attach Film for Stacked-Die Chip Scale Packages," J. Mater. Sci.: Mater. Electron., **27**(1), pp. 481–488.
[30] Tay, A. A. O., and Lin, T. Y., 1996, "Moisture Diffusion and Heat Transfer in Plastic IC Packages," IEEE Trans. on Components, Packing, and Manufacturing Technology, **19**(2), pp. 186–193.
[31] Wong, E. H., and Rajoo, R., 2003, "Moisture Absorption and Diffusion Characterisation of Packaging Materials—Advanced Treatment," Microelectron. Reliab., **43**(12), pp. 2087–2096.
[32] Wong, E. H., Koh, S. W., Lee, K. H., Lim, K. M., Lim, T. B., and Mai, Y. W., 2006, "Advances in Vapor Pressure Modeling for Electronic Packaging," IEEE Trans. Adv. Packag., **29**(4), pp. 751–759.
[33] Shi, Y., Tay, A. A. O., Wong, E. H., and Ranjan, R., 2002, "An Effective Method of Characterizing Moisture Desorption of Polymeric Materials at High Temperature," 4th Electronics Packaging Technology Conference (EPTC), Singapore, Dec. 10–12, pp. 70–75.
[34] Jang, C., Han, B., and Yoon, S., 2010, "Comprehensive Moisture Diffusion Characteristics of Epoxy Molding Compounds Over Solder Reflow Process Temperature," IEEE Trans. Compon. Packag. Technol., **33**(4), pp. 809–818.
[35] Jang, C., and Han, B., 2014, "Hygrothermal Behavior of Advanced Polymers Above Water Boiling Temperatures," ASME J. Electron. Packag., **136**(1), p. 011013.
[36] Vieth, W. R., Howell, J. M., and Hsieh, J. H., 1976, "Dual Sorption Theory," J. Membr. Sci., **1**, pp. 177–220.
[37] Fujita, H., 1961, "Diffusion in Polymer-Diluent Systems," *Fortschritte Der Hochpolymeren-Forschung*, Springer, Berlin.
[38] Berry, B. S., and Pritchet, W. C., 1984, "Bending-Cantilever Method for the Study of Moisture Swelling in Polymers," IBM J. Res. Dev., **28**(6), pp. 662–667.
[39] Xiao, G. Z., and Shanahan, M. E. R., 1998, "Swelling of DGEBA/DDA Epoxy Resin During Hygrothermal Ageing," Polymer, **39**(14), pp. 3253–3260.
[40] Buchhold, R., Nakladal, A., Gerlach, G., Sahre, K., Eichhorn, K.-J., and Müller, M., 1998, "Reduction of Mechanical Stress in Micromachined Components Caused by Humidity-Induced Volume Expansion of Polymer Layers," Microsyst. Technol., **5**(1), pp. 3–12.
[41] Post, D., Han, B., and Ifju, P., 1994, *High Sensitivity Moiré*, Springer-Verlag, New York.
[42] Sutton, M. A., McNeill, S. R., Helm, J. D., and Chao, Y. J., 2000, "Advances in Two-Dimensional and Three-Dimensional Computer Vision," *Photomechanics*, P. K. Rastogi, ed., Springer, Berlin.
[43] Stellrecht, E., Han, B., and Pecht, M., 2003, "Measurement of the Hygroscopic Swelling Coefficient in Mold Compounds Using Moiré Interferometry," Exp. Tech., **27**(4), pp. 40–44.
[44] Jang, C., Yoon, S., and Han, B., 2010, "Measurement of the Hygroscopic Swelling Coefficient of Thin Film Polymers Used in Semiconductor Packaging," IEEE Trans. Compon. Packag. Technol., **33**(2), pp. 340–346.
[45] Mikhaĭlov, M. D., and Özìsìk, M. N., 1984, *Unified Analysis and Solutions of Heat and Mass Diffusion*, Wiley, New York.
[46] Vaddadi, P., Nakamura, T., and Singh, R. P., 2003, "Inverse Analysis for Transient Moisture Diffusion Through Fiber-Reinforced Composites," Acta Mater., **51**(1), pp. 177–193.
[47] Wu, B., Yang, W., and Jia, C., 2004, "A Three-Dimensional Numerical Simulation of Transient Heat and Mass Transfer Inside a Single Rice Kernel During the Drying Process," Biosyst. Eng., **87**(2), pp. 191–200.
[48] Jang, C., and Han, B., 2009, "Analytical Solutions of Gas Transport Problems in Inorganic/Organic Hybrid Structures for Gas Barrier Applications," J. Appl. Phys., **105**(9), p. 093532.
[49] Jang, C., Cho, Y.-R., and Han, B., 2008, "Ideal Laminate Theory for Water Transport Analysis of Metal-Coated Polymer Films," Appl. Phys. Lett., **93**(13), p. 133307.
[50] Uschitsky, M., and Suhir, E., 1998, "Moisture Diffusion in Epoxy Molding Compounds Filled With Particles," ASME J. Electron. Packag., **123**(1), pp. 47–51.

[51] Puig, O., Martinot, C., and Roustan, P., 1998, "Moisture Ingress and Absorption in a CCD Package Characterisation, Modelisation and Measurement," POLY, Paris, France, pp. 1–7.
[52] Wong, E. H., Teo, Y. C., and Lim, T. B., 1998, "Moisture Diffusion and Vapor Pressure Modeling of IC Packaging," 38th Electronic Components and Technology Conference (ECTC), Seattle, WA, May 25–28, pp. 1372–1378.
[53] Wong, E. H., Chan, K. C., Tee, T. Y., and Rajoo, R., 1999, "Comprehensive Treatment of Moisture Induced Failure in IC Packaging," 3rd Electronics Manufacturing Technology Conference (IEEE), pp. 176–181.
[54] Wong, E. H., Koh, S. W., Lee, K. H., and Rajoo, R., 2002, "Comprehensive Treatment of Moisture Induced Failure-Recent Advances," IEEE Trans. Electron. Packag. Manuf., **25**(3), pp. 223–230.
[55] Wong, E. H., Rajoo, R., Koh, S. W., and Lim, T. B., 2002, "The Mechanics and Impact of Hygroscopic Swelling of Polymeric Materials in Electronic Packaging," ASME J. Electron. Packag., **124**(2), pp. 122–126.
[56] Wong, E. H., Koh, S. W., Lee, K. H., and Rajoo, R., 2002, "Advanced Moisture Diffusion Modeling and Characterisation for Electronic Packaging," 52nd Electronic Components and Technology Conference (ECTC), San Diego, CA, May 28–31, pp. 1297–1303.
[57] Chen, X., Zhao, S., and Zhai, L., 2005, "Moisture Absorption and Diffusion Characterization of Molding Compound," ASME J. Electron. Packag., **127**(4), pp. 460–465.
[58] Vogels, R. C. J., Huang, M., Yang, D. G., Driel, W. D. V., and Zhang, G. Q., 2005, "Fast Characterization for Moisture Properties of Moulding Compounds: Influence of Temperature and Humidity," 6th International Conference on Electronic Packaging Technology (EPT), Shenzhen, China, Aug. 30–Sept. 2, pp. 185–190.
[59] Chang, K.-C., Yeh, M.-K., and Chiang, K.-N., 2004, "Hygrothermal Stress Analysis of a Plastic Ball Grid Array Package During Solder Reflow," Proc. Inst. Mech. Eng., Part C, **218**(9), pp. 957–970.
[60] Tay, A. A. O., and Lin, T. Y., 1998, "Moisture-Induced Interfacial Delamination Growth in Plastic IC Packages During Solder Reflow," 48th IEEE Electronic Components and Technology Conference (ECTC), Seattle, WA, May 25–28, pp. 371–378.
[61] He, Y., and Fan, X. J., 2007, "In-Situ Characterization of Moisture Absorption and Desorption in a Thin BT Core Substrate," 57th Electronic Components and Technology Conference (ECTC), Reno, NV, May 29–June 1, pp. 1375–1383.
[62] Fan, X. J., and Suhir, E., 2010, *Moisture Sensitivity of Plastic Packages of IC Devices*, Springer, New York.
[63] Fan, X., and Jie-Hua, Z., 2011, "Moisture Diffusion and Integrated Stress Analysis in Encapsulated Microelectronics Devices," 12th International Conference on Thermal, Mechanical and Multi-Physics Simulation and Experiments in Microelectronics and Microsystems (EuroSimE), Linz, Austria, Apr. 18–20, pp. 1/8–8/8.
[64] He, Y., 2011, "In-Situ Characterization of Moisture Absorption-Desorption and Hygroscopic Swelling Behavior of an Underfill Material," IEEE 61st Electronic Components and Technology Conference, Orlando, FL, May 31–June 3, pp. 375–386.
[65] Jang, C., Goswami, A., and Han, B., 2009, "Hermeticity Evaluation of Polymer-Sealed MEMS Packages by Gas Diffusion Analysis," J. Microelectromech. Syst., **18**(3), pp. 577–587.
[66] Sarvar, F., Hutt, D. A., and Whalley, D. C., 2002, "Application of Adhesives in MEMS and MOEMS Assembly: A Review," POLYTRONIC 2nd International IEEE Conference on Polymers and Adhesives in Microelectronics and Photonics, Zalaegerszeg, Hungary, June 23–26, pp. 22–28.
[67] Niklaus, F., Stemme, G., Lu, J.-Q., and Gutmann, R. J., 2006, "Adhesive Wafer Bonding," J. Appl. Phys., **99**(3), p. 031101.
[68] Jourdain, A., Moor, P. D., Pamidighantam, S., and Tilmans, H. A. C., 2002, "Investigation of the Hermeticity of BCB-Sealed Cavities for Housing (RF-) MEMS Devices," The 15th IEEE International Conference on Micro Electro Mechanical Systems (MEMS), Las Vegas, Jan. 20–24, pp. 677–680.
[69] Noh, H., Kyoung-Sik, M., Cannon, A., Hesketh, P. J., and Wong, C. P., 2004, "Wafer Bonding Using Microwave Heating of Parylene for MEMS Packaging," 54th Electronic Components and Technology Conference (ECTC), Las Vegas, June 1–4, pp. 924–930.
[70] Jang, C., and Han, B., 2010, "Modeling of Moisture Diffusion and Moisture-Induced Stresses in Semiconductor and MEMS Packages," *Moisture Sensitivity of Plastic Packages of IC Devices*, X. J. Fan and E. Suhir, eds., Springer US, Boston, MA.
[71] Goswami, A., 2008, "Quantitative Hermeticity Assessment of Packages With Micro to Nano-Liter Cavities," Ph.D. dissertation, Mechanical Engineering, University of Maryland, College Park, MD.
[72] Jang, C., Goswami, A., Han, B., and Ham, S.-J., 2009, "In Situ Measurement of Gas Diffusion Properties of Polymeric Seals Used in MEMS Packages by Optical Gas Leak Testing," J. Micro/Nanolithogr., MEMS, MOEMS, **8**(4), p. 043025.